The International Journal of Advanced Manufacturing Technology (2018) 95:4607–4621
https://doi.org/10.1007/s00170-018-1581-1

ORIGINAL ARTICLE

Temperature prediction in Inconel 718 milling with microstructure evolution

Yixuan Feng[1] · Zhipeng Pan[1] · Steven Y. Liang[1]

Received: 30 August 2017 / Accepted: 11 December 2017 / Published online: 14 January 2018

Abstract
For this study, a new temperature prediction analytical model for Inconel 718 milling is presented with the consideration of microstructure evolution while accounting for the effects of dynamic recrystallization. The milling condition is transferred to equivalent orthogonal cutting condition at each rotation angle. The previous constant yield stress term in Johnson-Cook constitutive equation is replaced by a grain size-dependent term. The grain size is calculated according to dynamic recrystallization, a strain and temperature induced recrystallization process, through the recrystallized volume fraction by Johnson-Mehl-Avrami-Kolmogorov model. The temperature rise is due to the flow stress in shear zone considered as primary heat source and the secondary rubbing heat source between the tool tip and machined surface. The heat source density is calculated based on the cutting forces predicted from flow stress. The predicted temperature field is validated by numerical model in six cases and experimental measurements in ten cases from two papers, and improvements are observed through the comparison between proposed and conventional models.

Keywords Inconel 718 · Milling · Temperature · Microstructure

1 Introduction

Machining Inconel 718 has been an attracting interest for researchers due to its superior properties and availability in aerospace and automobile industries. High temperature and cutting forces always accompany the machining process. Therefore, it is valuable to predict the temperature in terms of optimized cutting parameters and extension of tool life. Ng et al. [1] did experiments on high-speed ball nose end milling of Inconel 718 and measured the average workpiece temperature. They found that a lower coefficient of friction on the rake face or a lower cutting speed would result in a reduction in cutting temperature. However, the physics inside the relationship between temperature and cutting parameters remained unknown at that time. Later, Özel et al. [2] predicted the temperature in high-speed flat end milling of P-20 mold steel through finite element method (FEM). The flow stress model was a constitutional model with microstructure evolution by involving temperature-dependent coefficients. The highest workpiece temperature was observed in the shear zone. The coefficients of constitutional model were calculated based on their experiments. Therefore, the numerical method was restricted to specific material and machining conditions, and the accuracy was harmed by uncertainty in flow stress model. Abukhshim et al. [3] reviewed the analytical models for the prediction of temperature in metal cutting and concluded that the current models were inaccurate due to the simplified assumptions such as the ignorance of microstructure evolution. Shi et al. [4] did numerical and experimental investigation in both conventional and laser-assisted machining of Inconel 718. Since the feed rate and the depth of cut were much smaller than the diameter of the cylindrical workpiece in their cases, the relative movement between the tool and workpiece was simplified as a translation. This assumption resulted in failure of temperature distribution prediction. Venkatesan et al. [5] also analyzed the temperature in Inconel 718 turning for optimal combination of cutting parameters. They

✉ Yixuan Feng
yfeng82@gatech.edu

[1] Woodruff School of Mechanical Engineering, Georgia Institute of Technology, Atlanta, GA 30332, USA

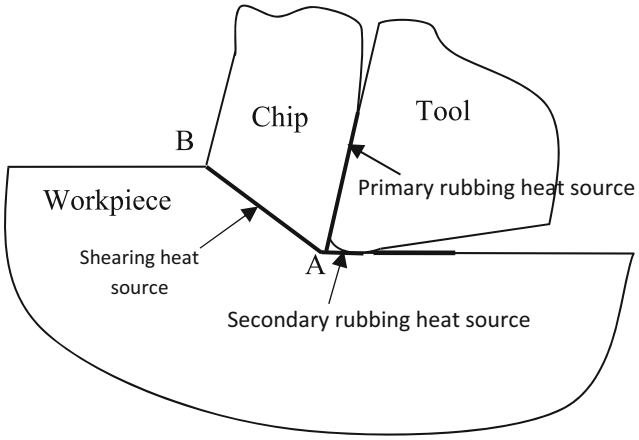

Fig. 1 Heat sources in Inconel 718 milling

applied the Taguchi method to design experiments and statistical analysis of variance for optimization. Since these methods were purely relied on experimental investigation, the conclusions were limited to observation and did not reflect physics nature. Le Coz et al. [6] used inserted thermocouples to measure the temperature variation in the workpiece during dry milling of Inconel 718 and collected the maximum temperature on the cutting edge under different cutting speed. In addition, Grzesik et al. [7] obtained the experimental data by high-speed infra-red camera, and the mean temperature between the rotation angle of 50° and 70° was listed under different cutting conditions. The experimental measurements from both two papers are compared with the prediction of proposed model in section 5.

Most works about temperature prediction in Inconel 718 milling so far are based on FEM or experimental investigation. One of the biggest limitations of analytical model is the simplified assumptions due to the complexity of milling process, and one major problem is the assumption of constant coefficients in constitutive law. The material properties of Inconel 718 are sensitive to microstructure evolution at high temperature. Therefore, it is essential to study and embed microstructure evolution into the analytical model. Huang et al. [8] summarized the recrystallization and grain growth models in commercial FEM code DEFORM. Dynamic recrystallization (DRX) occurs during deformation when the critical strain is reached. Static recrystallization (SRX) or metadynamic recrystallization (MRX) will occur after deformation when the imposed strain is less or greater than the critical strain. All the other researchers have studied on recrystallization [9–11] and concluded that DRX is the main microstructure evolution during Inconel 718 milling. The body-centered tetragonal γ''-Ni3Nb precipitates and face-centered cubic γ'-Ni3(Al, Ti) precipitates are the two main phases in Inconel 718. Because of the high volume fraction of the γ'' and γ' strengthening precipitates, high yield strength under high temperature is observed. The flow stress is related to yield stress according to the Johnson-Cook constitutive model. The flow stress is then highly dependent on microstructure. Therefore, a modified Johnson-Cook flow stress model is able to catch the possible DRX in the shear zone [12]. The augmented grain size under different temperature is predicted through dynamically recrystallized grain size and recrystallized volume fraction [13], and the grain size-dependent yield strength is calculated through the inverse relationship between the grain diameter and stress for dislocation movement [14]. The proposed temperature prediction method is introduced in section 2. The microstructure evolution is described in section 3. The comparison between the proposed analytical model and numerical model is discussed in section 4. Moreover, the comparison between the proposed method and experimental data from literature is presented in section 5.

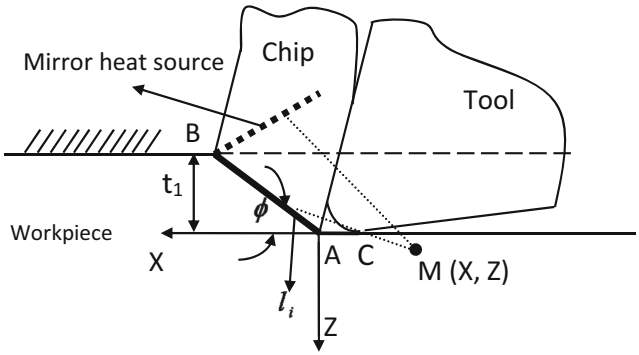

Fig. 2 Schematic of the primary heat source for workpiece

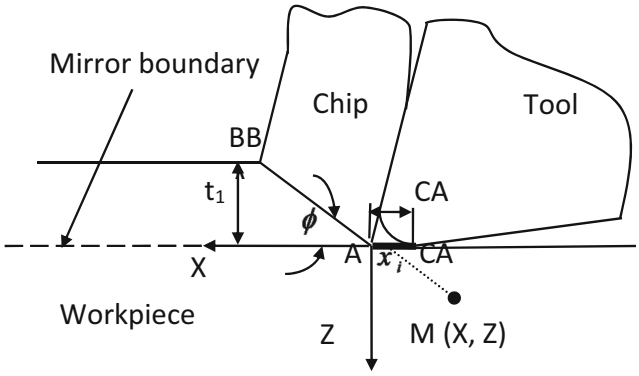

Fig. 3 Schematic of the rubbing heat source for workpiece

Table 1 A modified Johnson-Cook model parameters for Inconel 718 [15]

A_{hp}(MPa)	K_{hp} (MPa$\sqrt{\mu m}$)	B(MPa)	C	m	n	T_m(°C)	$\dot{\varepsilon}_0$ (s^{-1})
378	298.4	1370	0.02	1.03	0.164	1300	1

Table 2 Inconel 718 material constants of JMAK model [8, 16, 17]

Peak strain	$a_1 d_0^{h1}$	m_1	$Q_{act}m_1$(J/mol)	c_1		
	0.4659×10^{-2}	0.1238	49,520	0		
DRX kinematics	β_d	k_d	a_{10}	a_2		
	0.693	2	0.8	0.8		
Required strain	a_5	h_5	n_5	m_5	$Q_{act}m_5$(J/mol)	c_5
	5.043×10^{-9}	0	−1.42	−0.408	196,000	0
DRX grain size	a_8	h_8	n_8	m_8	$Q_{act}m_8$(J/mol)	c_8
	4.85×10^{10}	0	−0.4	−0.028	−240,000	0

2 Analytical modeling of temperature prediction

At each rotation angle, the milling process is simplified as an orthogonal cutting process. The equivalent side cutting angle, chip flow angle, inclination angle, rake angle, cutting depth, and cutting speed are transferred based on the milling condition. The cutting force F_c and the radial force F_t are then predicted in modified Oxley's model. The transformation and force prediction are presented in previous work [14]. The presented temperature prediction model estimates the temperature rise from three heat sources, the shear heat source at shear zone due to shearing deformation, the primary rubbing heat source due to the friction on tool-chip interface, and the secondary rubbing heat source between tool tip and machined surface. The heat sources in Inconel 718 milling are shown in Fig. 1. The primary rubbing heat source contributes to the temperature rise of chip instead of workpiece, so only the other two heat sources are predicted. Both the heat sources are assumed moving, and the uncut workpiece surface is assumed to be adiabatic. Therefore, a mirror heat source method is applied to predict temperature rise.

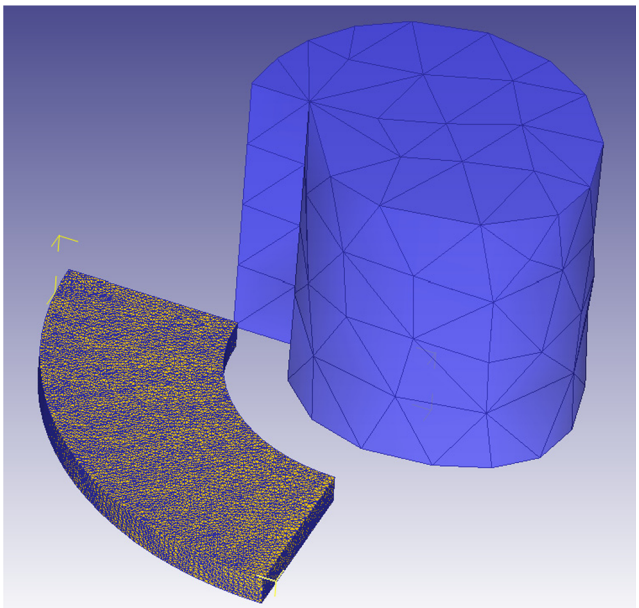

Fig. 4 Geometry and mesh of workpiece and tool

Figure 2 shows the primary heat source of workpiece due to the plastic shearing deformation in shear zone. Any point on workpiece $M(X, Z)$ is under a temperature rise from shearing heat source and its mirror heat source. The temperature rise at point M is calculated by:

$$\left.\begin{aligned}\Delta T_{wk-shear}(X,Z) &= \frac{q_{shear}}{2\pi k_{wk}}\int_0^{L_{AB}} e^{-\frac{(X-l_i\sin\phi)V}{2a_{wk}}}\left\{K_0\left[\frac{V}{2a_{wk}}\sqrt{(X-l_i\cos\phi)^2+(Z+l_i\sin\phi)^2}\right]\right.\\ &\left.+K_0\left[\frac{V}{2a_{wk}}\sqrt{(X-l_i\cos\phi)^2+(2t_1-l_i\sin\phi+Z)^2}\right]\right\}dl_i\end{aligned}\right. \quad (1)$$

where $L_{AB}=\frac{t_1}{\sin\phi}$ is the length of shear plane, t_1 is the uncut chip thickness, ϕ is the shear angle, k_{wk} is the thermal conductivity, a_{wk} is the thermal diffusivity, K_0 is the modified Bessel function of the second kind or Neumann function, V is the cutting speed, and q_{shear} is the shear plane heat density calculated by:

$$q_{shear}=\frac{(F_c\cos\varphi-F_t\sin\varphi)(V\cos\alpha/\cos(\varphi-\alpha))}{t_1\cdot w\cdot\csc\varphi} \quad (2)$$

where F_c is the tangential cutting force, F_t is the radial cutting force, α is the rake angle, and w is the cutting width.

Similarly, the secondary heat source between the tool tip and the machined surface from rubbing is treated as a moving heat source along= X direction as illustrated in Fig. 3. The temperature rise due to the rubbing is calculated as:

$$\Delta T_{wk-rub}(X,Z) = \frac{q_{rub}}{\pi k_{wk}}\int_0^{CA}\gamma e^{-\frac{(-X-x_i)V}{2a_{wk}}}\left\{K_0\left(\frac{V}{2a_{wk}}\sqrt{(X+x_i)^2+Z^2}\right)\right\}dx_i \quad (3)$$

Table 3 The mechanical and thermal properties of Inconel 718 [18] and tungsten carbide

Properties	Value (Inconel 718)	Value (tungsten carbide)
Young's modulus	− 74.35 T + 214,790 MPa	560,000 MPa
Poisson's ratio	0.3	0.3
Thermal expansion	$10^{-5}\ e^{0.0004T/^{\circ}C}$	
Thermal conductivity	11.367 $e^{0.0009T}$ W/m · k	84.02 W/m · k
Heat capacity	418.63 $e^{0.0433T}$ J/(Kg·°C)	500 J/(Kg·°C)
Emissivity	0.8	
Density	8.19 g/cm^3	15.8 g/cm^3

where CA is the contact length and q_{rub} is the secondary rubbing heat source density calculated by:

$$q_{rub} = \frac{P_{cut}V}{w \cdot CA} \tag{4}$$

where P_{cut} is the plowing force in cutting direction. γ is a heat distribution coefficient defined as:

$$\gamma = \frac{\sqrt{k_{wk}\rho_{wk}C_p}}{\sqrt{k_{wk}\rho_{wk}C_p} + \sqrt{k_t\rho_tC_t}} \tag{5}$$

where k_{wk}, p, C, k_t, p_t, and C_t are the thermal conductivity, density, and specific heat of the workpiece and cutting tool respectively. Therefore, the temperature rise of any point on the workpiece $M(X, Z)$ is calculated as the summation of two temperature rise sources,

$$\Delta T_{total}(X,Z) = \Delta T_{wk-shear}(X,Z) + \Delta T_{wk-rub}(X,Z) \tag{6}$$

3 Microstructure evolution modeling

The cutting forces predicted in Eq. (2) are based on the modified Johnson-Cook constitutive law during the calculation of flow stress. The conventional Johnson-Cook equation $\sigma = (A + B\bar{\varepsilon}^n)\left(1 + C\ln\frac{\dot{\bar{\varepsilon}}}{\dot{\bar{\varepsilon}}_0}\right)\left\{1-\left(\frac{T-T_0}{T_m-T_0}\right)^m\right\}$ has a constant initial yield stress A. In the proposed model, the Hall-Petch equation is applied to describe the relationship between yield stress and grain size:

$$A = A_{hp} + K_{hp}d^{-0.5} \tag{7}$$

where A is the yield stress of Inconel 718, d is the average grain size, and A_{hp} and K_{hp} are material constants. The modified Johnson-Cook flow stress equation becomes:

$$\sigma = \left(A_{hp} + K_{hp}d^{-0.5} + B\bar{\varepsilon}^n\right)\left(1 + C\ln\frac{\dot{\bar{\varepsilon}}}{\dot{\bar{\varepsilon}}_0}\right)\left\{1-\left(\frac{T-T_0}{T_m-T_0}\right)^m\right\} \tag{8}$$

where B, C, m, and n are still material constants as listed in Table 1, $\bar{\varepsilon}$ is the plastic strain, $\dot{\bar{\varepsilon}}$ is the plastic

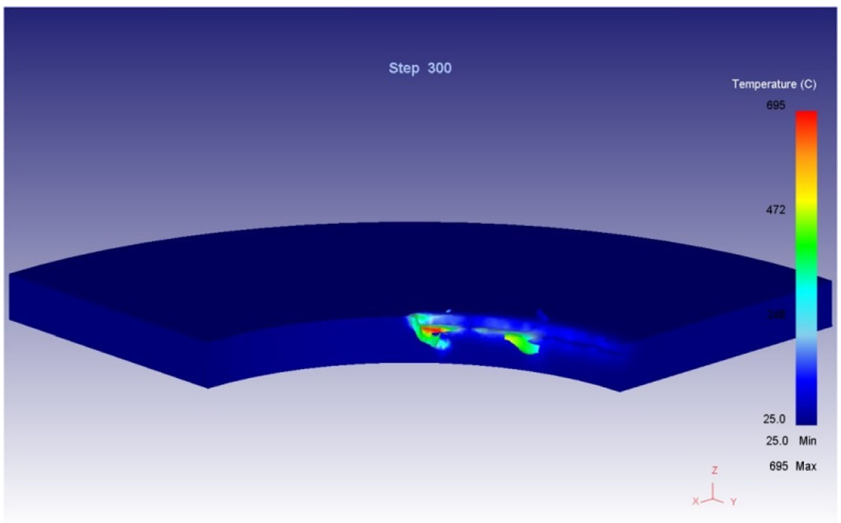

Fig. 5 Simulated temperature field at a feed rate of 200 mm/min, an axial depth of milling of 0.1 mm

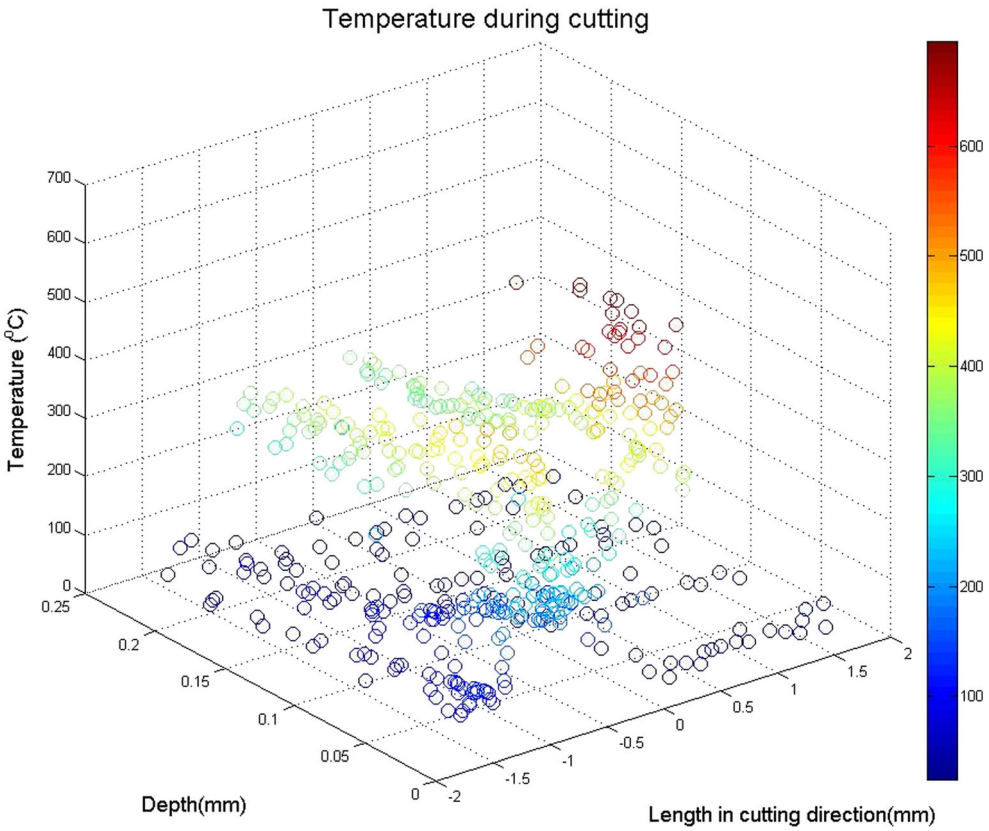

Fig. 6 Temperature measurement data from numerical model at a feed rate of 200 mm/min, an axial depth of milling of 0.1 mm

strain rate, $\dot{\bar{\varepsilon}}_0$ is the reference strain rate, assumed to be 1 s^{-1}, T_m is the melting temperature of Inconel 718, T_0 is the environment temperature, and T is the temperature of interested area. The values of modified Johnson-Cook flow stress model parameters are from Jafarian et al. [15] in Table 1.

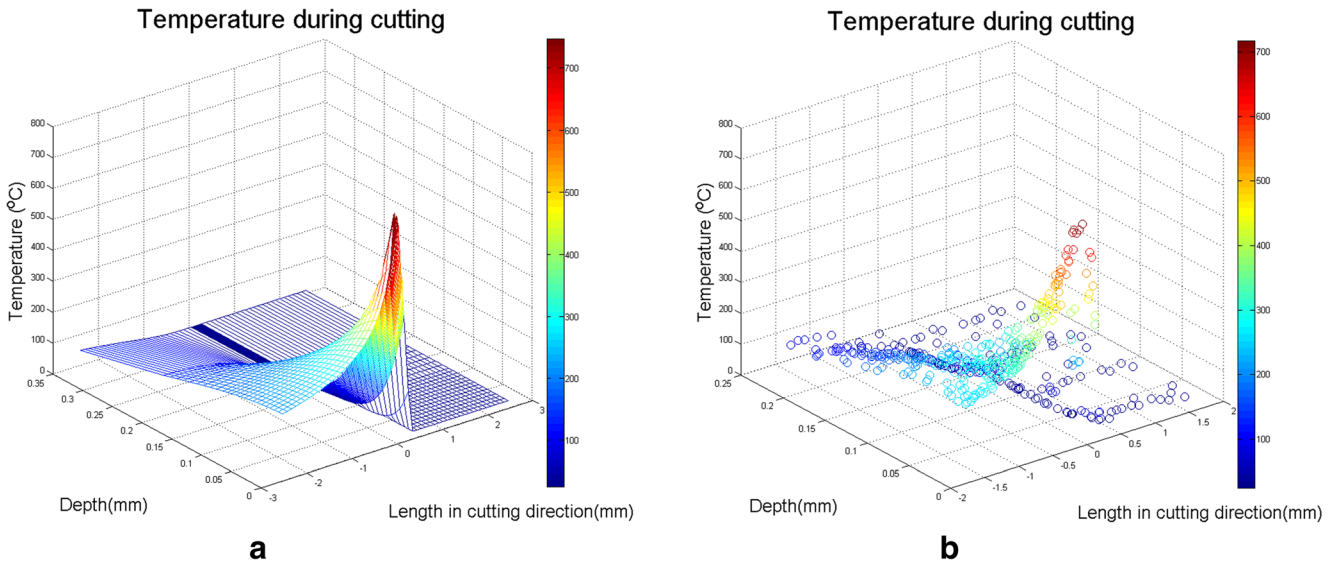

Fig. 7 Analytical predictions without DRX process (**a**) before and (**b**) after interpolation at a feed rate of 200 mm/min, an axial depth of milling of 0.1 mm

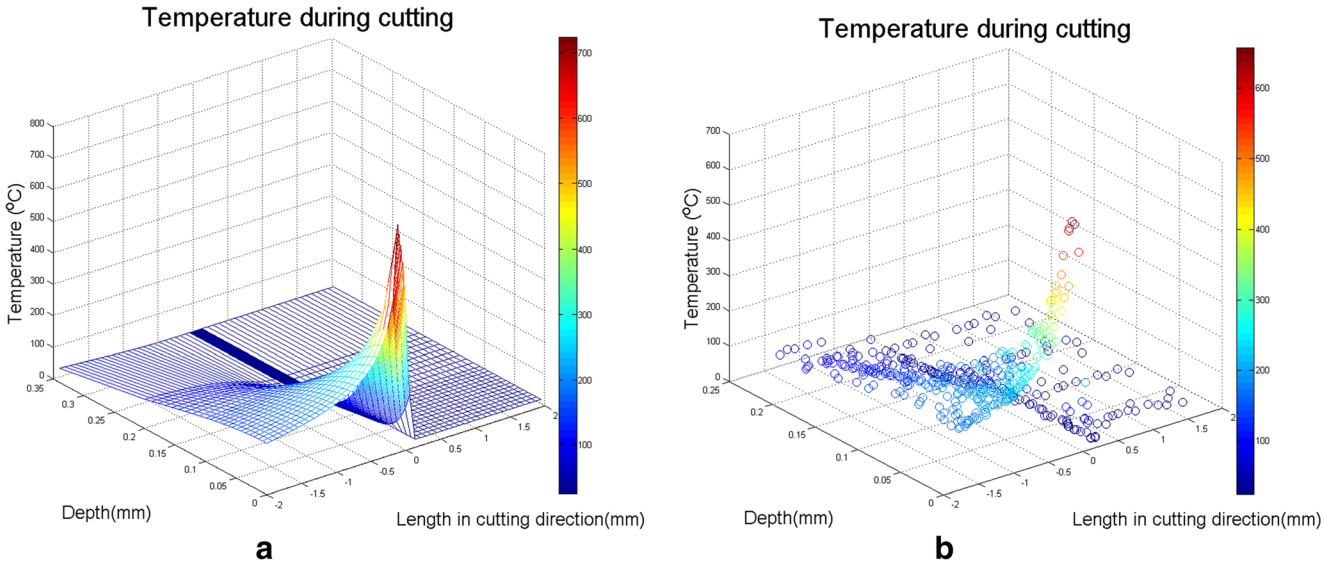

Fig. 8 Analytical predictions with DRX process (**a**) before and (**b**) after interpolation at a feed rate of 200 mm/min, an axial depth of milling of 0.1 mm

For the prediction of average grain size d, the JMAK model is applied to simulate the DRX process. Assumption is made that nucleation and grain growth are randomly distributed on the workpiece, and the average grain size d is expressed as:

$$d = d_{drex}X_{drex} + d_0(1-X_{drex}) \tag{9}$$

where d_0 is the initial grain size of Inconel 718, assumed to be 10 μm, d_{drex} is the average grain size after DRX, and X_{drex} is the recrystallized volume fraction. As long as the plastic strain $\bar{\varepsilon}$ exceeds a predefined threshold value $a_2\varepsilon_p$, the dynamic recrystallization process starts. The recrystallized volume fraction X_{drex} is defined by the Avrami equation:

$$X_{drex} = 1-\exp\left[-\beta_d\left(\frac{\bar{\varepsilon}-a_{10}\varepsilon_p}{\varepsilon_{0.5}}\right)^{k_d}\right] \tag{10}$$

where ε_p is the peak strain calculated by:

$$\varepsilon_p = a_1 d_o^{\,h_1}\dot{\bar{\varepsilon}}_0^{\,m_1}\exp(Q_{act}m_1/RT) + c_1 \tag{11}$$

R is the gas constant, Q_{act} is the activation energy, and $\varepsilon_{0.5}$ is the corresponding strain when 50% of the grain

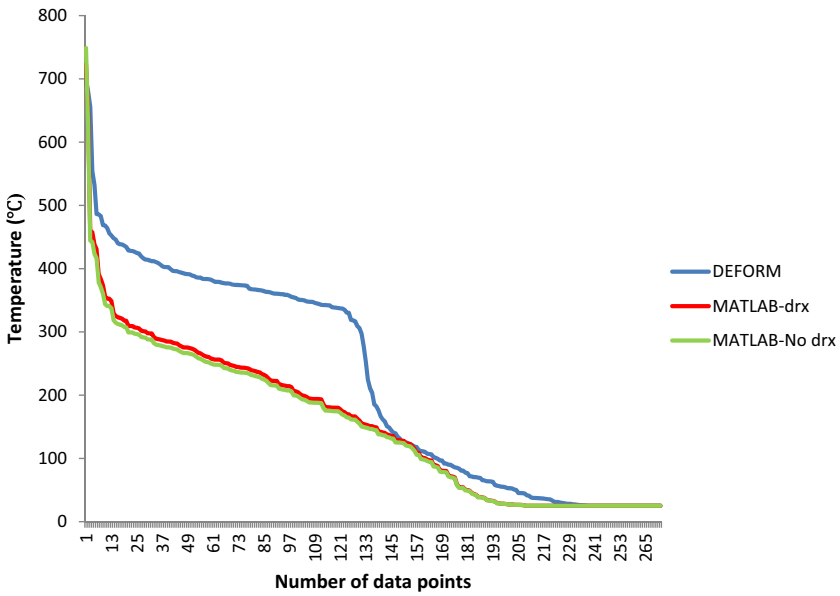

Fig. 9 Temperature measurements of all data points from DEFORM and MATLAB at a feed rate of 200 mm/min, an axial depth of milling of 0.1 mm

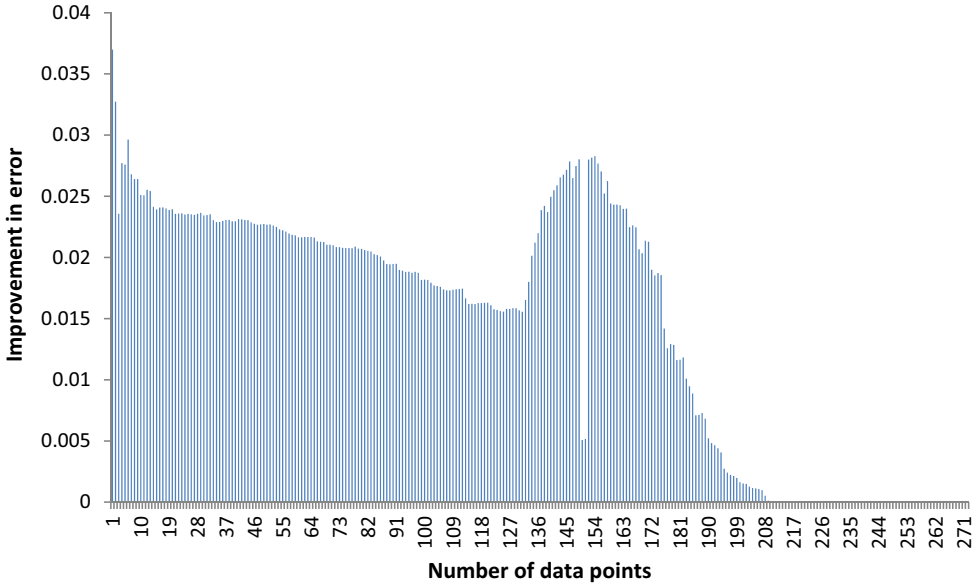

Fig. 10 Percentage improvement of proposed analytical model at all temperature data points at a feed rate of 200 mm/min, an axial depth of milling of 0.1 mm

is dynamically recrystallized or $X_{drex} = 0.5$, $\varepsilon_{0.5}$ is calculated as:

$$\varepsilon_{0.5} = a_5 d_0^{h_5} \bar{\varepsilon}^{n_5} \dot{\bar{\varepsilon}}^{m_5} \exp(Q_{act} m_5 / RT) + c_5 \quad (12)$$

The average grain size after *DRX* or d_{drex} is decided by:

$$d_{drex} = a_8 d_0^{h_8} \bar{\varepsilon}^{n_8} \dot{\bar{\varepsilon}}^{m_8} \exp(Q_{act} m_8 / RT) + c_8 \quad (13)$$

All the coefficients from Eqs. (10) to (13) including a_{10}, β_d, and k_d in Eq. (10), a_1, h_1, m_1, and c_1 in Eq. (11), a_5, h_5, n_5, m_5, and c_5 in Eq. (12), and a_8, h_8, n_8, m_8, and c_8 in Eq. (13) are material constants listed in Table 2. These JMAK model parameters are referred from Huang et al. [8], Reyes et al. [16], and Loyda et al. [17].

4 Numerical validation

The proposed analytical model is validated in both numerical and experimental methods. The numerical validation is conducted by FEM in DEFORM v11.1. The Inconel 718 workpiece has a sector shape with 0.5-mm thickness, 3-mm width, and 3-mm inner radius as shown in Fig. 4. The material of milling tool is tungsten carbide with one flute. The thermal

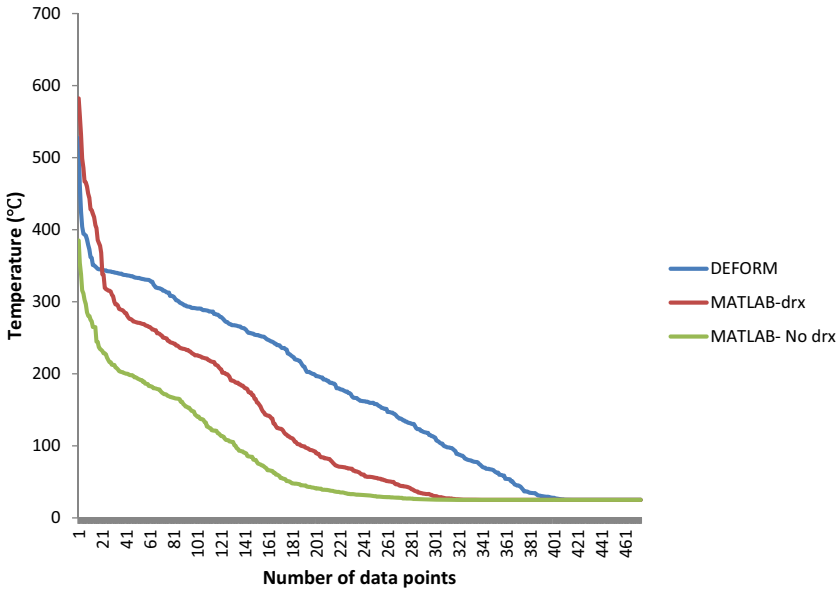

Fig. 11 Temperature measurements of all data points from DEFORM and MATLAB at a feed rate of 200 mm/min, an axial depth of milling of 0.15 mm

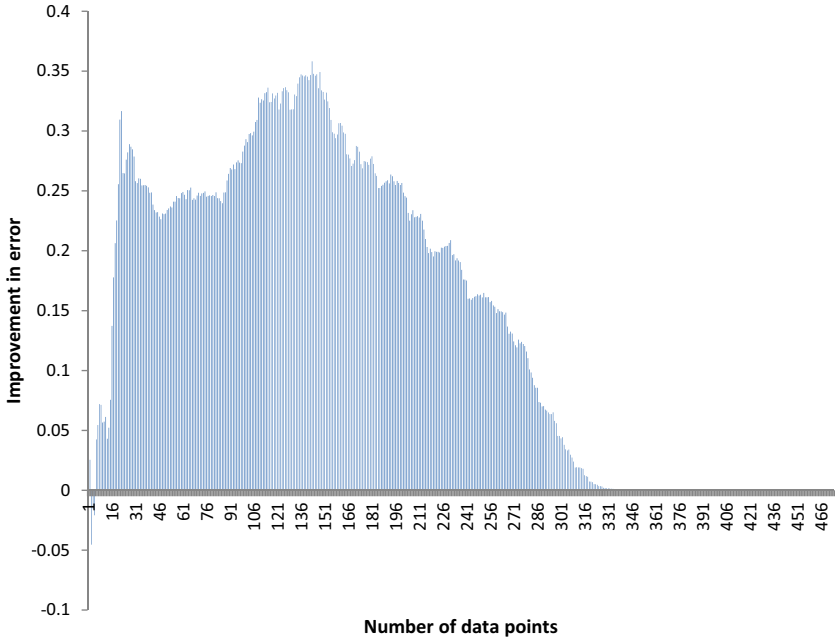

Fig. 12 Percentage improvement of proposed analytical model at all temperature data points at a feed rate of 200 mm/min, an axial depth of milling of 0.15 mm

and mechanical properties of both materials are listed in Table 3. The spindle speed is selected to be 3000 rpm, the rake angle is 35°, the inclination angle is 15°, the side cutting angle is 45°, the tool radius is 3 mm, and the nose radius is 0.1 mm. The workpiece has a convection coefficient of 0.02 N/s mm°C with the environment, in which the temperature is 25°C. The constitutive model is described by the Johnson-Cook equation. Six cases are simulated based on two different feed rates, 200 or 300 mm/min, and three different axial depth of milling, 0.1, 0.15, or 0.2 mm. The number of elements on workpiece is 97,128, and the element number of milling tool is 985. The tool is rotating with 100 π rad/s of angular velocity in counter clockwise, and the translation movement is set up based on the feed rate. The milling process is simulated for rotation angle between 0 and 180°. The computation time for each step varies from 90 to 150 s with a total step number between 672 and 1171 for six cases. The predicted temperature distribution is compared with simulation results at a rotation angle of 45°.

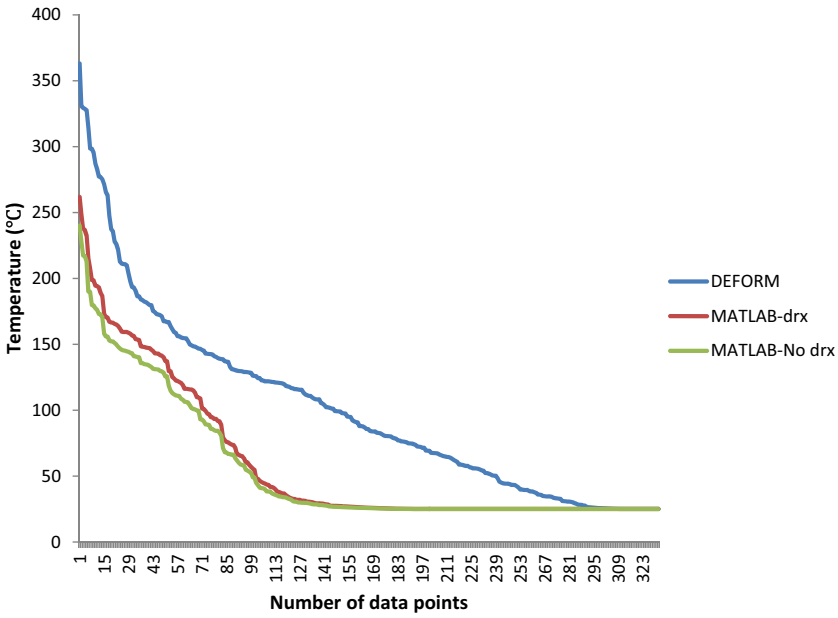

Fig. 13 Temperature measurements of all data points from DEFORM and MATLAB at a feed rate of 200 mm/min, an axial depth of milling of 0.2 mm

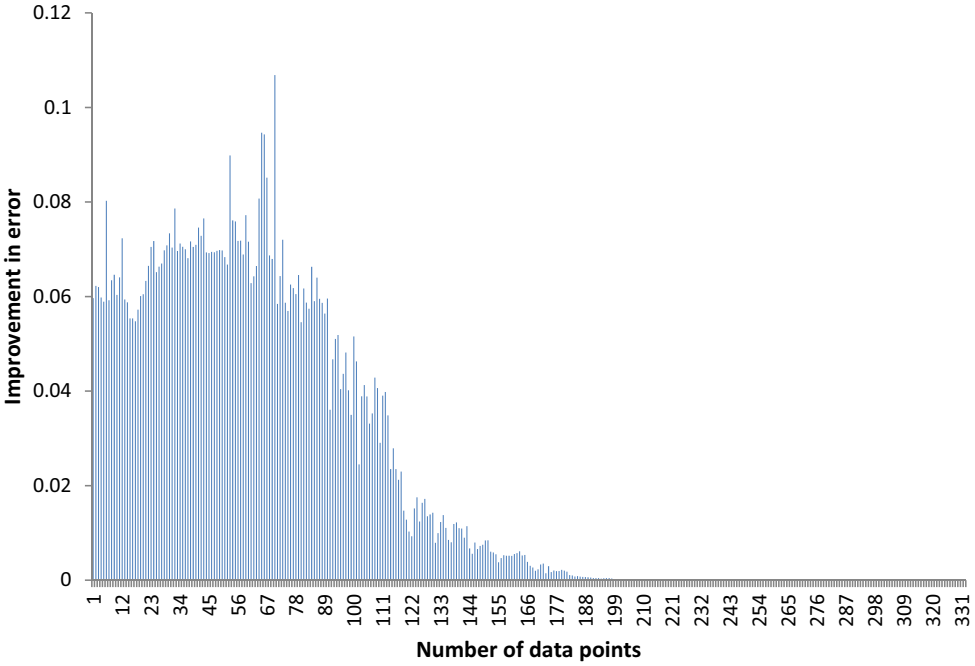

Fig. 14 Percentage improvement of proposed analytical model at all temperature data points at a feed rate of 200 mm/min, an axial depth of milling of 0.2 mm

The simulated temperature field at 45° rotation angle on the workpiece is shown in Fig. 5, when the feed rate is 200 mm/min and the axial depth of milling is 0.1 mm. Based on the coordinate system defined in Figs. 2 and 3, the proposed analytical model predicts the temperature distribution within 1.75 mm > X > − 1.795 mm and 0.34 mm > Z > 0.0001 mm. Since 100 data points and 26 data points are evenly selected in X and Z directions, there are total of 2600 temperature data points collected from analytical model. The simulated temperature field outside of this range is eliminated with 272 remaining nodes matching the analytical results. The 272 temperature measurements from FEM are plotted in Fig. 6. The temperature data from analytical model is then interpolated to find temperature at same position in numerical model. The interpolation process takes four data points around to get temperature at corresponding position with the distances as weigh coefficients. The analytical predictions without DRX process before and after interpolation are shown in Fig. 7. The analytical predictions with DRX process before and after interpolation are shown in Fig. 8. After the interpolation process, the temperature prediction from both methods has the same number of data points. The temperature measurements

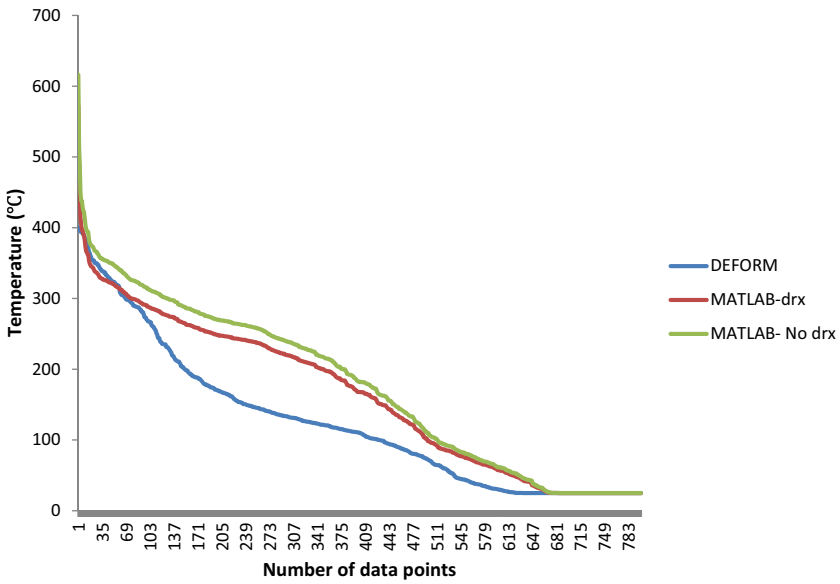

Fig. 15 Temperature measurements of all data points from DEFORM and MATLAB at a feed rate of 300 mm/min, an axial depth of milling of 0.1 mm

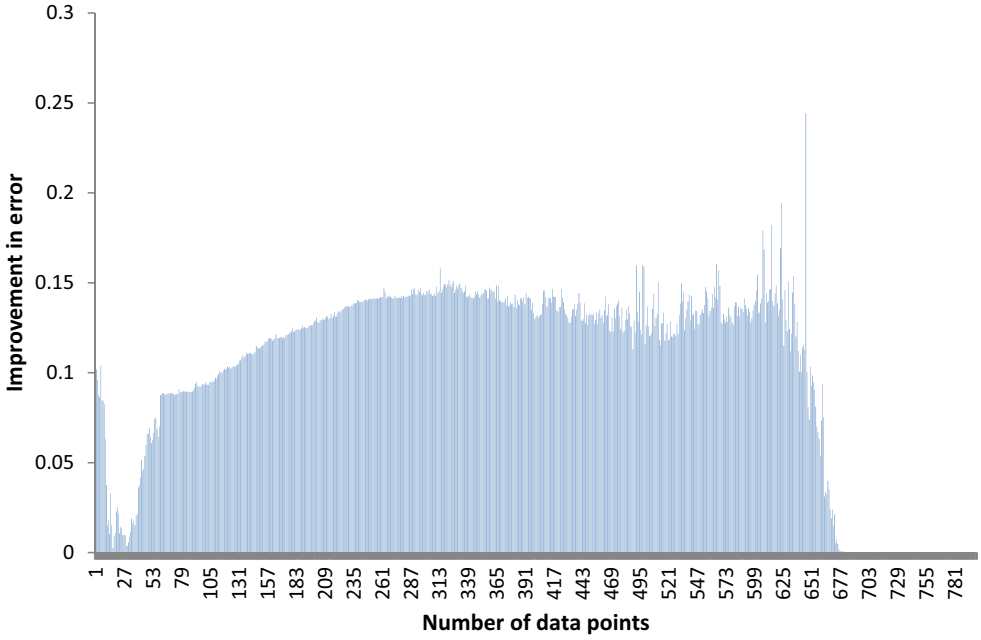

Fig. 16 Percentage improvement of proposed analytical model at all temperature data points at a feed rate of 300 mm/min, an axial depth of milling of 0.1 mm

from DEFORM, MATLAB with DRX process, and MATLAB without DRX process are plotted in Fig. 9. As shown in Fig. 9, the temperature distribution from analytical model follows the same trend as the numerical results with the highest temperature about 700°C. In addition, it is clear that the proposed analytical model provides a closer distribution comparing to the previous model without DRX process. To further demonstrate the accuracy of proposed model, for every data point, both percentage error between numerical model and proposed analytical model with microstructure evolution and percentage error between numerical model and previous analytical model without microstructure evolution are calculated. Figure 10 shows the improvement in percentage error at each corresponding data point. The proposed temperature prediction model has better accuracy in all data points with about 3% less error in general.

The same process is repeated for the remaining five cases. For case two, the feed rate remains 200 mm/min while the axial depth of milling increases to 0.15 mm. The analytical model predicts temperature distribution within the same depth range of 0.34 mm > Z > 0.0001 mm but different range of 1.008 mm > X > −1.037 mm in cutting direction since the boundaries of X coordinates are relevant to the chip-tool contact length for each case. After selection, 474 nodes from numerical model are inside these boundaries. The

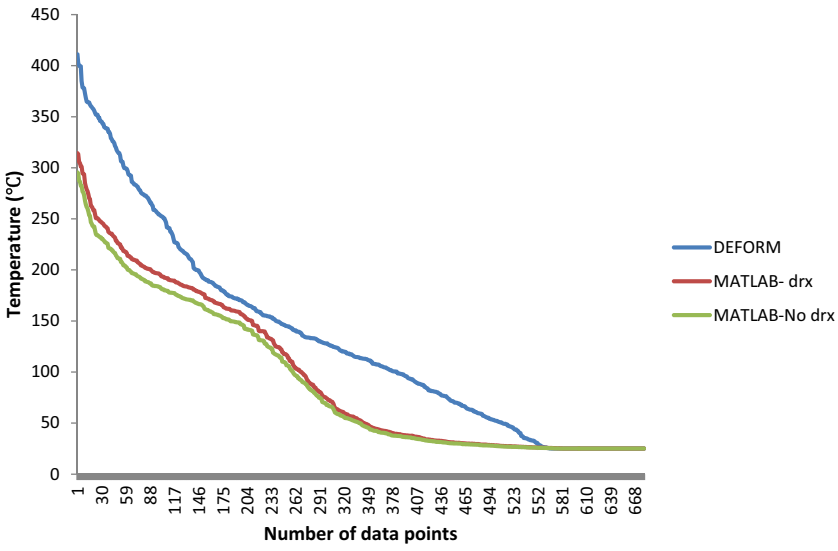

Fig. 17 Temperature measurements of all data points from DEFORM and MATLAB at a feed rate of 300 mm/min, an axial depth of milling of 0.15 mm

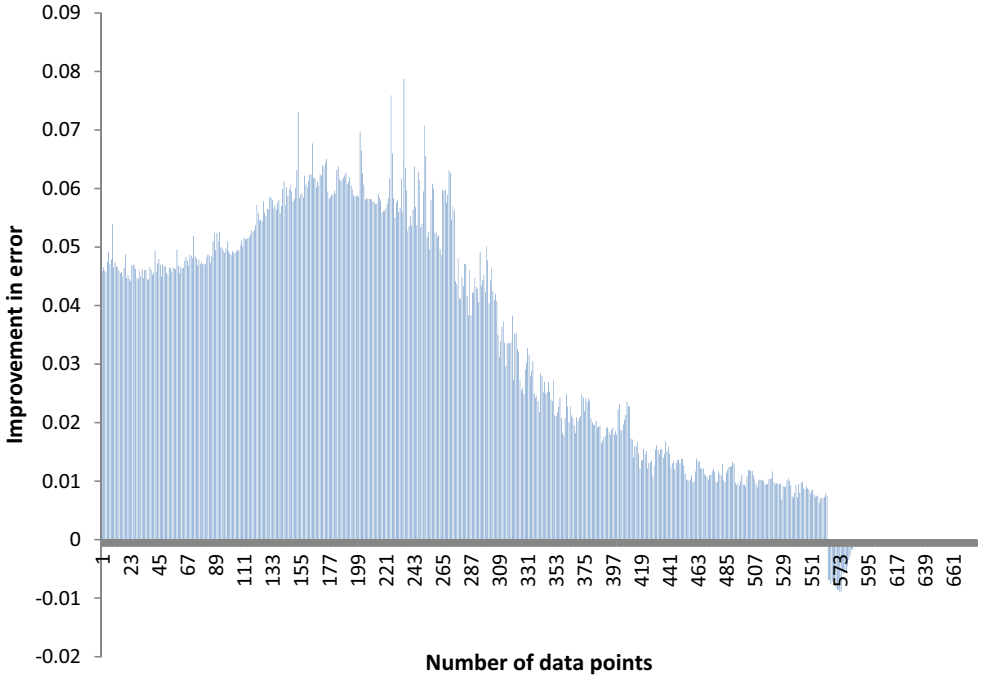

Fig. 18 Percentage improvement of proposed analytical model at all temperature data points at a feed rate of 300 mm/min, an axial depth of milling of 0.15 mm

temperature measurements from DEFORM, MATLAB with DRX process, and MATLAB without DRX process are plotted in Fig. 11. Moreover, the improvement in percentage error at each corresponding data point is shown in Fig. 12. It is noticed that the proposed temperature prediction model has better accuracy with 35% less error at some points.

Feed rate is 200 mm/min and axial depth of milling is 0.2 mm for case three. For both analytical model with or without DRX process, 2600 data points are collected within $0.785\ \text{mm} > X > -0.808\ \text{mm}$ and $0.34\ \text{mm} > Z > 0.0001\ \text{mm}$. After interpolation, 332 data points are calculated to match the simulation results. Figure 13 represents the temperature measurements from DEFORM and two models from MATLAB. Again, the proposed model has a better guess especially for the first 150 data points. The error gap plot in Fig. 14 confirms this conclusion with the biggest improvement over 10%.

For case four, the feed rate jumps to 300 mm/min with an axial depth of milling of 0.1 mm. FEM provides 801 nodes within the range of $2.077\ \text{mm} > X > -2.137\ \text{mm}$ and $0.34\ \text{mm} > Z > 0.0001\ \text{mm}$. Both analytical models predict temperature higher than simulation as shown in Fig. 15, but

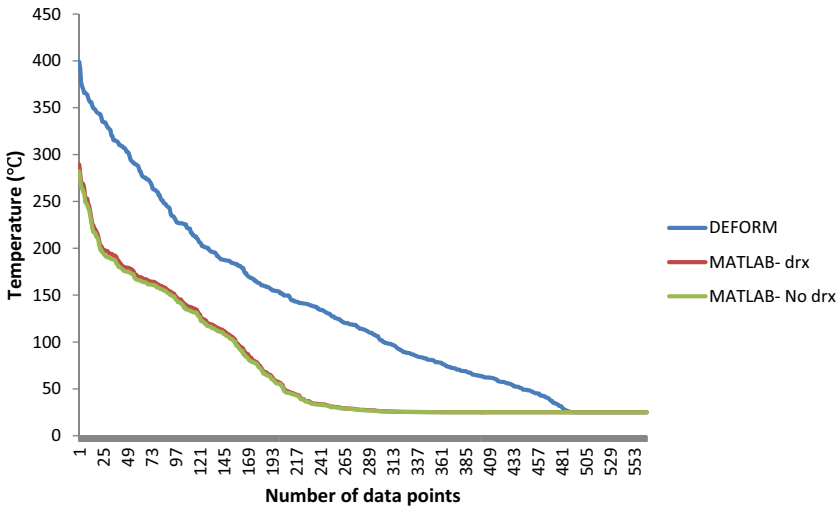

Fig. 19 Temperature measurements of all data points from DEFORM and MATLAB at a feed rate of 300 mm/min, an axial depth of milling of 0.2 mm

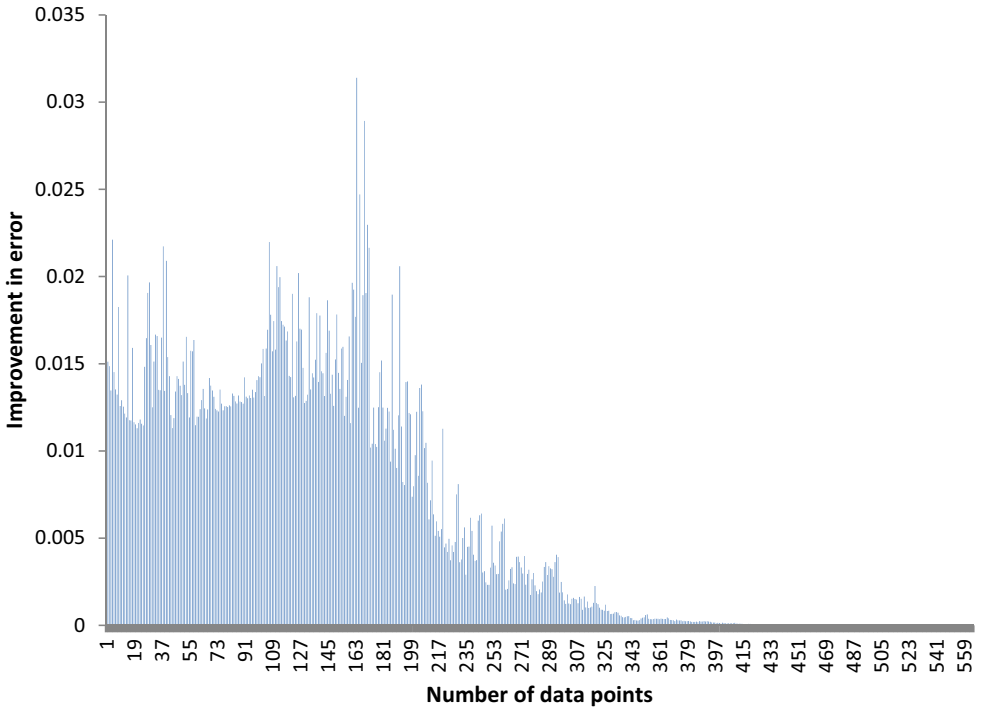

Fig. 20 Percentage improvement of proposed analytical model at all temperature data points at a feed rate of 300 mm/min, an axial depth of milling of 0.2 mm

the proposed model is still more accurate with lower temperature. From Fig. 16, most data points have a more than 10% less error with peak value over 20%.

Under the same feed rate of 300 mm/min, the cutting depth is 0.15 mm for case five and 0.2 mm for case six. Same observations are found from trend plot in Fig. 17 with a maximum accuracy improvement over 7% in Fig. 18 for case five. The prediction results from two analytical models are quite similar for case six as shown in Fig. 19. But with microstructure evolution, the proposed model is still slightly better with 1 to 3% improvement as shown in Fig. 20.

The improvement of proposed model is further demonstrated from the comparison of highest measured temperature in each case as listed in Table 4. The peak temperature decreases with the increase of axial depth of milling. The proposed analytical predicts higher temperature for case one, two, and four, and lower temperature at larger axial depth of milling. However, the temperature prediction model with microstructure evolution is always more accurate than the previous model in terms of highest temperature in all six cases.

5 Experimental validation

The proposed temperature prediction model is also validated by comparing predictions with experimental results from existing literature. Le Coz et al. [6] predicted the temperature variation in the workpiece when dry milling Inconel 718. The experiments were carried out on a high-speed machining center Roeders RP600. The workpieces were mounted on a piezoelectric dynamometer Kistler 9265B to measure the cutting forces during the process. The signal was amplified by a charge amplifier Kistler 5017B and recorded by a multichannel acquisition device Dewetron DEWE2010. The axial depth of cut was 8 mm. The feed per tooth was 0.07 mm, the spindle speed or cutting speed was 40, 60, 80, 160, and 320 m/min,

Table 4 Highest temperature (°C) measured in numerical and analytical models (V_f indicates the feed rate in mm/min, doc indicates the axial depth of milling in mm)

	DEFORM	MATLAB: without dynamic recrystallization	MATLAB: with dynamic recrystallization
$V_f = 200$ doc = 0.1	695	748	723
$V_f = 200$ doc = 0.15	527	384	582
$V_f = 200$ doc = 0.2	363	240	262
$V_f = 300$ doc = 0.1	401	616	572
$V_f = 300$ doc = 0.15	411	295	314
$V_f = 300$ doc = 0.2	399	282	289

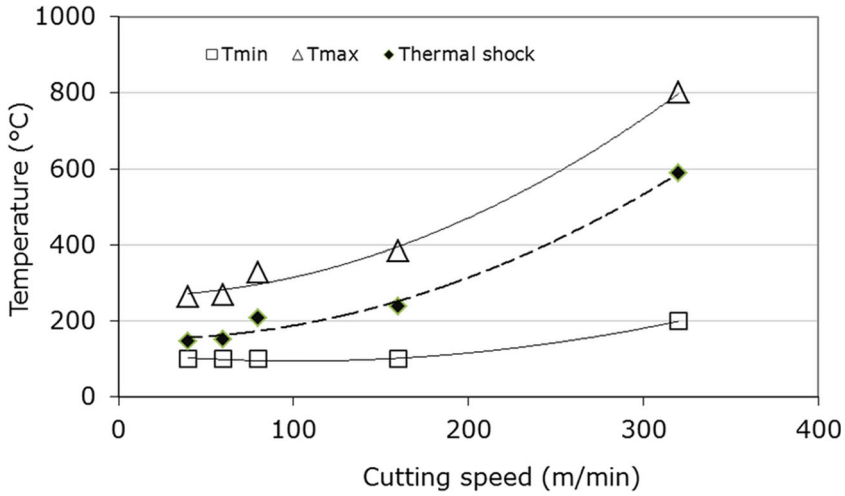

Fig. 21 Evolution of T_{min}, T_{max}, and thermal shock with cutting speed [6]

the tool diameter was 16 mm, and the teeth number was two. The tool was a PVD TiAlN multilayer-coated carbide insert (grade GC1030). Figure 21 shows the maximum and minimum temperature as well as the thermal shock measured under different cutting speed. As listed in Table 5, both analytical models predict the trend correctly. The highest temperature increases with the increases of cutting speed. The proposed model including DRX process provides more accurate results at first four cases, especially when the cutting speed is 60 or 80 m/min.

Grzesik et al. [7] created a numerical model to predict milling temperature at different rotation angle as shown in Fig. 22. The tests were carried out for a flat milling with tree-flute cutter-head type KSSR050RN12CF03 with SiAlON inserts type RNGN120700E KY1540 from KENNAMETAL. The milling machine was CNC DMU 80P duoBLOCK equipped with an HD infra-red camera, model X6540sc. Five combinations were selected from the depth of cut of 1, 1.5, and 2 mm, feed per tooth of 0.1, 0.125, and 0.15 mm, and cutting speed of 750 and 800 m/min. The tool diameter was 10 mm and the tooth number was three. The region with maximum temperature corresponds to the rotation angle between 50 and 70°, so the mean values of cutting temperature were measured as mean temperature in Table 6 for this machining period. The temperature was predicted at a rotation angle of 60° in proposed model. As shown in Table 6, the measured temperature increases with a larger cutting depth or feed per tooth. The proposed model with microstructure evolution shows a better match for case three and five, where the conventional model has a drop in predicted temperature. The proposed model also predicts a closer temperature under a cutting depth of 1 mm and feed rate of 0.15 mm/tooth, since the previous model has a much higher prediction. Both models are in good agreement with experiments in the other two conditions, but the new model still shows improvements over 5%. The average error for the proposed model is 4% with a maximum error of 9.2%, while the error of conventional model is 24% with a maximum error of 44%.

6 Conclusion

For this study, a new temperature prediction analytical model for Inconel 718 milling is presented with microstructure evolution. The milling condition is transferred to equivalent orthogonal cutting condition at each rotation angle. The cutting forces and plowing forces are then calculated based on modified Oxley's model with the modified Johnson-Cook flow stress law. The previous constant yield stress term in the Johnson-Cook equation is replaced by grain size-dependent

Table 5 Comparison of highest temperature (°C) between analytical models and experimental results from Le Coz et al. [6] with an axial depth of cut of 8 mm and feed per tooth of 0.07 mm

Spindle speed (m/min)	40	60	80	160	320
T_{max} (with dynamic recrystallization)	240.52	286.03	325.14	463.05	714.64
T_{max} (no dynamic recrystallization)	360.55	321.25	364.01	516.25	794.70
T_{max} (literature)	270	280	330	390	800

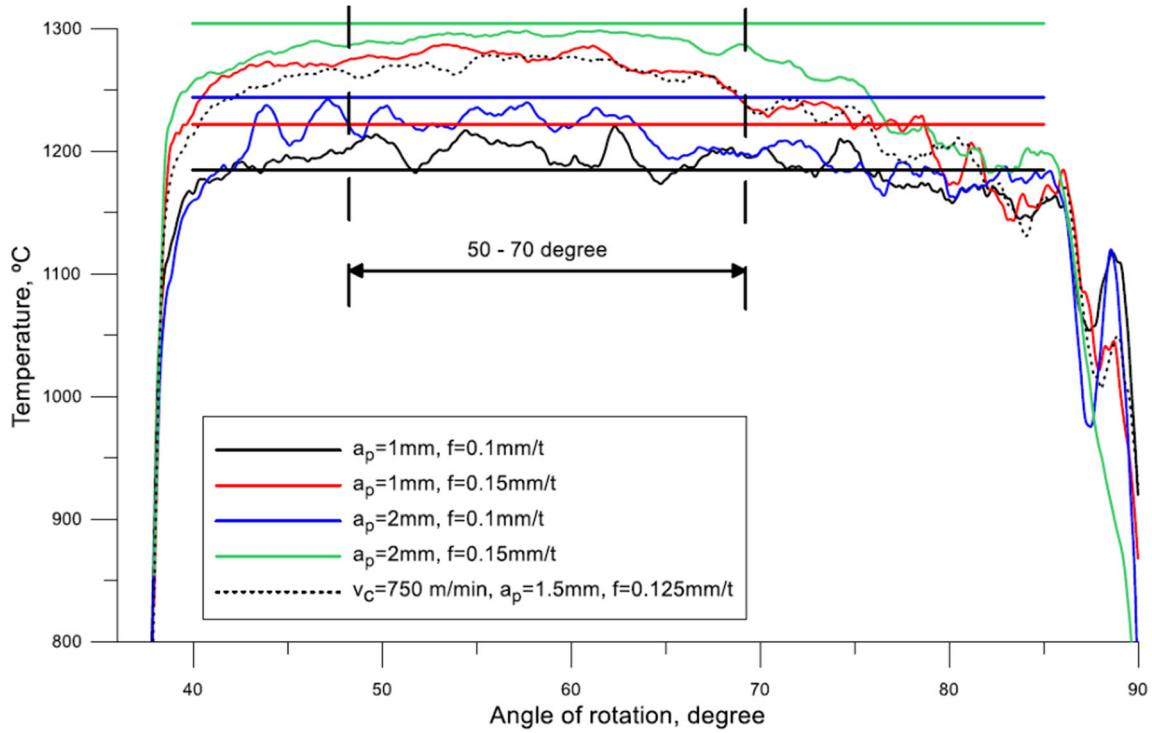

Fig. 22 Comparison of simulated cutting temperatures with minimum values of measured temperature (lines parallel to the *X* axis). Machining parameters: $v_c = 800$ and 750 m/min (only dotted line), $a_p = 1$ and 2 mm, $f = 0.1$ and 0.15 mm/tooth [7]

term through the Hall-Petch equation. The grain size is calculated according to DRX process, a strain and temperature-induced recrystallization process, by JMAK model. When the plastic strain exceeds the threshold value, the recrystallized volume fraction is calculated, and the augmented grain reduces flow stress. The temperature rise is predicted from the primary heat source in shear zone and the secondary rubbing heat source between the tool tip and machined surface. Through the predicted cutting and plowing forces, the heat source density is calculated, and the mirror heat source method provides the way of integration of heat density along shear plane or rubbing surface.

The predicted temperature field is validated by numerical model in six cases and experimental measurements in ten cases from two papers, and the following conclusions are drawn:

- DRX process is the main microstructure evolution occurred during Inconel 718 milling.
- The proposed temperature prediction model provides closer temperature distribution to numerical model in all six cases with a maximum improvement over 35%.
- The proposed temperature prediction model provides more accurate highest temperature prediction in all cases from numerical model, and nine out of ten cases from experimental measurements.

The proposed model is valuable in terms of providing a more accurate analytical method in temperature prediction of Inconel 718 milling. The predicted temperature is more accurate by 35% when compared with FEM simulation, and 20% when compared with experimental measurements. The future work will focus on the other recrystallization process

Table 6 Comparison of highest temperature (°C) between analytical models and experimental results from Grzesik et al. [7]

Cutting speed m/min	Cutting depth mm	Feed per tooth mm	Mean temperature	Analytical model with DRX	Analytical model without DRX
800	1.0	0.10	1236	1232	1327
800	1.0	0.15	1268	1175	1824
800	2.0	0.10	1286	1322	855
800	2.0	0.15	1374	1381	1208
750	1.5	0.125	1293	1174	996

including SRX or MRX that occurs in Inconel 718 milling in order to include all forms of microstructure evolution for better accuracy.

References

1. Ng E-G, Lee DW, Sharman ARC, Dewes RC, Aspinwall DK, Vigneau J (2000) High speed ball nose end milling of Inconel718. CIRP Ann Manuf Technol 49(1):41–46. https://doi.org/10.1016/S0007-8506(07)62892-3
2. Özel T, Altan T (2000) Process simulation using finite element method—prediction of cutting forces, tool stresses and temperatures in high-speed flat end milling. Int J Mach Tool Manu 40(5):713–738. https://doi.org/10.1016/S0890-6955(99)00080-2
3. Abukhshim NA, Mativenga PT, Sheikh MA (2006) Heat generation and temperature prediction in metal cutting: a review and implications for high speed machining. Int J Mach Tools Manuf 46(7–8):782–800. https://doi.org/10.1016/j.ijmachtools.2005.07.024
4. Shi B, Attia H, Vargas R, Tavakoli S (2008) Numerical and experimental investigation of laser-assisted machining of Inconel 718. Mach Sci Technol 12(4):498–513. https://doi.org/10.1080/10910340802523314
5. Venkatesan K, Ramanujam R, Kuppan P (2014) Analysis of cutting forces and temperature in laser assisted machining of Inconel 718 using Taguchi method. Procedia Eng 97:1637–1646. https://doi.org/10.1016/j.proeng.2014.12.314
6. Le Coz G, Dudzinski D (2014) Temperature variation in the workpiece and in the cutting tool when dry milling Inconel 718. Int J Adv Manuf Technol 74(5-8):1133–1139. https://doi.org/10.1007/s00170-014-6006-1
7. Grzesik W et al (2015) Influence of cutting conditions on temperature distribution in face milling of Inconel 718 nickel-chromium alloy. J Mach Eng 15(2):5–16
8. Huang D et al (2001) Computer simulation of microstructure evolution during hot forging of Waspaloy and nickel alloy 718
9. Robert P, Guest ST (2005) The dynamic and metadynamic recrystallisation of in 718. p. 373–383
10. Wang Y et al (2007) Investigation on dynamic recrystallization behavior in hot deformed Superalloy Inconel 718. Mater Sci Forum 546-549:1297–1300. https://doi.org/10.4028/www.scientific.net/MSF.546-549.1297
11. Azarbarmas M, Aghaie-Khafri M, Cabrera JM, Calvo J (2016) Dynamic recrystallization mechanisms and twining evolution during hot deformation of Inconel 718. Mater Sci Eng A 678:137–152. https://doi.org/10.1016/j.msea.2016.09.100
12. Pan Z, Feng Y, Liang SY (2017) Material microstructure affected machining: a review. Manuf Rev 4:5. https://doi.org/10.1051/mfreview/2017004
13. Pan Z et al (2017) Microstructure-sensitive flow stress modeling for force prediction in laser assisted milling of Inconel 718. Manuf Rev 4:6. https://doi.org/10.1051/mfreview/2017005
14. Pan Z et al (2017) Force modeling of Inconel 718 laser-assisted end milling under recrystallization effects. Int J Adv Manuf Technol 92(5-8):2965–2974. https://doi.org/10.1007/s00170-017-0379-x
15. Jafarian F, Imaz Ciaran M, Umbrello D, Arrazola PJ, Filice L, Amirabadi H (2014) Finite element simulation of machining Inconel 718 alloy including microstructure changes. Int J Mech Sci 88:110–121. https://doi.org/10.1016/j.ijmecsci.2014.08.007
16. Reyes LA, Páramo P, Salas Zamarripa A, de la Garza M, Guerrero-Mata MP (2016) Influence of processing parameters on grain size evolution of a forged superalloy. J Mater Eng Perform 25(1):179–187. https://doi.org/10.1007/s11665-015-1828-z
17. Loyda A, Hernández-Muñoz GM, Reyes LA, Zambrano-Robledo P (2016) Microstructure modeling of a Ni-Fe-based superalloy during the rotary forging process. J Mater Eng Perform 25(6):2128–2137. https://doi.org/10.1007/s11665-016-2104-6
18. Arrazola PJ, Kortabarria A, Madariaga A, Esnaola JA, Fernandez E, Cappellini C, Ulutan D, Özel T (2014) On the machining induced residual stresses in IN718 nickel-based alloy: experiments and predictions with finite element simulation. Simul Model Pract Theory 41:87–103. https://doi.org/10.1016/j.simpat.2013.11.009